PREPARATION OF DUAL FLUORESCENCE AGENTS-LOADED NANOPARTICLE AND ITS *IN VITRO* AND *IN VIVO* APPLICATION

By

HONG-HOA THI VU

THESIS

Submitted in partial fulfillment of the requirements for the degree of Master of Science in Bioengineer at The University of Texas at Arlington

December 2018

Arlington, Texas

Supervising Committee:

Liping Tang

Yi Hong

He Dong

Table of Contents

List of Figure

ACKNOWLEDGEMENTS

This project would not be possible without the support from many people. First, many thanks to my advisor, Dr. Liping Tang, who gave me the opportunity to perform my master project at his lab in the University of Texas at Arlington; Dr. Tang also read numerous copies of my revisions as well as gave great advice. Thanks to my supervisor, Dr. Jun Zhou. It was a pleasure to be able to work along-side with him, and gain knowledge throughout the experimental period. His critical advises and feedbacks helped me to continuously improve this project even at tough points. Moreover, many thanks to my colleagues, who contributed greatly to this project. YiHui Huang and Amirhossein Hakamivala from Bioengineering Department, helped me perform my experiment as well as collect images data for in vivo and in vitro studies, respectively. Min Khang from also Bioengineering and Chemistry Department, helped me obtain Transmission electron microscopy images. Without them, this project would not be thoroughly completed. Thanks to the University of Texas at Arlington, for providing resources that allow me to research this study and allow to me to learn throughout this process. Finally, thanks to my family and friends, who endured and gave me support and love.

ABSTRACT

PREPARATION OF DUAL FLUORESCENCE AGENTS-LOADED NANOPARTICLE AND ITS *IN VITRO* AND *IN VIVO* APPLICATION

Hong-Hoa Thi Vu, Master's Degree The University of Texas at Arlington, 2018

Supervising Professor: Liping Tang

There're many existing imaging tools that composed of different imaging moieties to improve both resolution and sensitivity, however there's not yet any imaging method that could be effectively utilized in both in vitro and in vivo study. To fill the gap, dual dyes-labeling fluorescent imaging nanoprobes was synthesized to simultaneous carry both visible fluorescent isothiocyanate (FITC) dye and near infra red (NIR) dye, 1,1′,3,3,3′,3′-hexamethylindotricarbocyanine iodide dye agent (HITC). For that, nanoparticles (NPs) was synthesized from 2-Hydroxyethyl methacrylate, styrene, acrylic acid and fluorescein-o-acrylate which contains visible FITC dye. The NPs were then labeled with HITC dye via physical entrapment to procedure HITC-FITC NPs. These nanoparticles have average size of 142.9nm±2.2, with high HITC loading efficiency (>90%). Our results confirm that both FITC and HITC dyes were successfully incorporated into NPs with high fluorescent intensity in both visible and NIR ranges. We have also observed possible static quenching effect caused by high concentrations of both dyes, whereas concentration of HITC increases reduce fluorescent intensity of FITC in NPs. By varying dye concentrations and ratios, we are able to fabricate HICT-FITC NPs with significant intensities in both NIR and visible ranges, with HITC/NPs weight ratio of 4X 10-4. Our results also confirmed that HICT-FITC NPs exhibits high photostability and colloid stability, as well as high aqueous-stability overtime. These particles

also have low cytotoxicity with cancer cells, with upper limit concentration of 0.3mg/ml. With this particle concentration, different types of cells, esophageal, prostate, fibroblast and macrophage cell, were labeled and high resolution cell images was able to produce by microscope at visible light channel. Finally, particles labeled cancer cells was able to be monitored in animal model under near infra-red range imaging

Introduction

Cell and biological molecules imaging in both *in vitro* and *in vivo* provide a great insight to how each component works and interacts.[1,2,3] In recent years, biological imaging field grew rapidly with new methods to improve sensitivity and quality image resolution. Most recent discoveries are Magnetic Resonance Imaging (MRI), Computed Tomography (CT), Positron Emission Tomography (PET), and optical imaging. Each method has its own advantage and limitation. NMR, CT and PET are commonly used in clinical setting because if their unlimitedness in tissues depth, however, low sensitivity while high in toxicity and instrumental expenses are their disadvantages[4] . On the other hand, despite of highly promising of its high sensitivity and low cost for microscopy imaging, optical cell labeling agents have limited utility for *in vivo* animal imaging due to their poor tissue penetration depth.[5,6] It is generally believing that multi-imaging modality agents would provide high sensitivity and accuracy as well as simpler experimental procedures to translate from cell study *in vitro* experiment to animal study *in vivo* experiment. Based on this assumption, many new imaging modalities have been developed to combine different imagining techniques in effort to compensate each other's advantages and disadvantages. Optical/MRI dual imaging nanoprobes were fabricated from glycol chitosan to exhibit high sensitivity and resolution *in vivo* imaging[7]. Similarly, dual imaging probe was synthesized by mesoporous silica nanoparticle conjugating europium and gadolinium ions for both *in vitro* and *in vivo* imaging. Although this nanoprobe gives high contrast imaging in both fields, it lacks sensitivity while exhibit high toxicity. Recently, quantum dots were extensively used as imaging probes in cell and animal studies; however, they tend to have high multi-valency and high cytotoxicity.[8,9] To the best of our knowledge, no biocompatible optical imaging probe has been developed to permit simultaneously whole body NIR imaging and optical microscopic examination.

To fill the gap, this study's objective is to design a biocompatible optical probe that is suitable for both *in vitro* and *in vivo* study using visible and near infrared (NIR) fluorescence. There's a variety of fluorescence agents which are detectable at different wavelengths and suitable for either *in vitro* or *in vivo* study[10]. For *in vivo* imaging, fluorescence dye agents at NIR wavelength (from 700nm to 1000 nm), including cyanine, rhodamine and porphyrin, have been used to gives high contrast resolution with minimal background fluorescence.[11] On the other hand, fluorescent dye agents in visible range, such as diaminophenyl-indole (DAPI), Hoechst or fluorescein (FITC), are highly desirable for microscopic imaging and observation.[12] Thus, by incorporating both types of fluorescence agents, a new cell labeling probe may be developed for both *in vitro* and *in vivo* imaging. It should be noted that, to obtain high accuracy and specificity in both fields, the difference in detectable wavelength of chosen dye agents must be as far from each other as possible to avoid interference or also known as quenching.[13] Based on these criteria, we have chosen FITC and 1,1′,3,3,3′,3′-hexamethylindotricarbocyanine iodide (HITC iodide) for this investigation. FITC (excitation wavelength = 495nm, emission wavelength = 519nm) is widely used for labeling nanoparticle, bacteria as well as antigen for *in vitro* imaging.[14,15,16] HITC iodide (excitation wavelength = 756nm, emission wavelength =776nm) has been widely used as a cell membrane labeling agent for in vivo animal imaging.[17,18]

These two fluorescence agents, FITC and HITC iodide were incorporated into imaging nanoprobe via two different methods. FITC is first chemically conjugated to the nanoparticles by introducing FITC-o-acrylate monomer during polymerization process. The HITC iodide is then embedded into the nanoparticles via physical adsorption using a polymer swelling procedure. These two agents are stabilized in particle form, which is composed of 2-Hydroxyethyl

Methacrylate (HEMA), styrene (St), Divinylbenzene (DVB) and acrylic acid. The purpose of hydrophobic styrene is to induce particle formation as well as fluorophore encapsulation[19]. On the other hand, hydrophilic HEMA, a biocompatible polymer, was shown to reduce toxicity in nanoparticle[20]. The nanoparticle is held together by crossing linker DVB. While acrylic acid helps stabilize particle by enhancing colloidal stability as well as allowing further surface modification[21]. We then determine the optical properties, stability and cell compatibility of the new cell labeling probe. Finally, using both *in vivo* and *in vivo* models, we evaluated this new imaging nanoprobe's ability to permit cell labeling in visible range and whole-body imaging in near infrared range.

Methodology

1. Materials

All materials were purchased in Sigma-Aldrich, unless indicate otherwise. Fluorescein-o-acrylate (M_W=386g/mol, FITC-acrylate), 2-Hydroxyethyl Methacrylate (M_W=130g/mol, HEMA), styrene (M_W=104g/mol, ST), Divinylbenzene (M_W=130g/mol, DVB), acrylic acid (M_W=72g/mol, AAc). Sodium dodecyl sulfate (SDS), Ammonium persulfate (APS), 1,1′,3,3,3′,3′-hexamethylindotricarbocyanine iodide (HITC iodide), tetrahydrofuran (THF), Dimethyl sulfoxide (DMSO). Hydrochloric acid, sodium hydroxide. NIH 3T3 murine fibroblast cells, Dulbecco's modified Eagle's medium (DMEM; Gibco, Thermo Fischer Scientific, Waltham, MA), fetal bovine serum. KYSE 30 esophageal cancer cells, Ham's F-10 medium and RPMI medium (both from Thermo Fischer Scientific).

2. HITC-FITC NPs preparation

2.1 Synthesis of FITC-NPs via step-wise emulsion polymerization

FITC-NPs are synthesized using a polymerization procedure (Scheme *1*) as previously reported.[22] Briefly, FITC-acrylate (0.036mmole), ST (14.8mmole), with crosslinker DVB (0.2mmole) and SDS (50mg) were added in Erlenmeyer flask with 70ml of distill water. The mixture was magnetically stirred under nitrogen gas and was place in circulating water bath at temperature of 75°C. To initiate polymerization, 5ml of APS (0.043mM) water was added after 20 minutes and reaction was run for an hour. Afterward, HEMA (4mmole) and AAc (1mmole) was mixed in separate vial and was added dropwise in the reaction flask. The reaction was allowed to run for another 2 hours. Dialysis was then performed to remove excess reagents. Purified nanoparticles' size was analyzed through Dynamic Light Scattering (DLS) with Mircotrac's Nanotrac UPA 1500 (Montgomeryville, PA). Morphology of the particle was analyzed by Transmission Electron Microscope H-9500 (Hitachi, Japan). Zeta potential of NPs was measured using NanoBrook Omni (Brookhaven Instruments Corporation, Holtsville, NY). To confirm chemical composition of NPs, Fourier-transform infrared spectroscopy (FTIR) was performed by Thermo Nicolet 6700 FTIR Spectrometer (Waltham, MA). Fluorescence intensity of FITC was also measured by Infinite M200 PRO Multimode Microplate Reader (Tecan, Switzerland). NP sample with highest intensity was selected for HITC iodide encapsulation and further analyzation. In addition, NPs without FITC-acrylate was also synthesized to use as control in photostability test.

2.2 Encapsulation of HITC iodide into FITC-NPs via dwelling effect

Loading of HITC iodide into the FITC-NPs was carried out as previously describe[13] and depicted in Scheme 2. 5ml of FITC-NPs solution (10mg/ml in distill water) was mixed with various amount

(2.5, 10, 40, 160, 640 and 1280 μL) of HITC iodide solution (0.5 mg/ml in THF). Additional THF was added to each sample to have total volume of 10mL. Samples were shaken in the dark and at room temperature for 24 hours. Then THF was removed by evaporation for another 24 hours. Samples were then purified by dialysis for at least 3 days, and then the dual dye-labelling probes (denoted as HITC-FITC NPs). Change in particle size was measured with DLS. Fluorescent emission and excitation scan were performed for FITC and HITC iodide using fluorescence microplate reader. Maximum emission and excitation wavelengths were determined and used to measure fluorescent intensity. Intensity was normalized by probe concentration. The sample with highest intensity in both ranges was selected as optimal patch for further analyzation. NPs without FITC-acrylate was also labeled with HITC to use as control in photostability test.

3. HITC-FITC NPs characterization

3.1 Quantification of carboxyl group on NPs surface via conductivity titration

Purified HITC-FITC-NPs was diluted to 10mg/ml with volume of 20mL. Excess 0.1M HCl was added for complete ionization of any base group. Then sample was titrated with 0.01M NaOH and conductivity was monitored by a Five Easy Conductivity Bench Meter Plus (Mettler-Toledo LLC, Columbus, OH). Carboxyl group was calculated from 2 equivalent points of titration curve[23].

3.2 HITC iodide loading efficiency via absorbance

For HITC iodide loading efficiency, similar procedure for HITC iodide loading (procedure 2.2) was performed except without dialysis. Instead, FITC-NPs and unloaded dye were separated by centrifuge. Filtrate that contained unloaded agent was collected and measure their absorbance was measured at wavelength of 740nm using DU 640 Spectrometer (Beckman, Fullerton, CA).

Calibration curve of HITC iodide in THF/water was created to calculate amount of unloaded dye and alternatively loading efficiency of HITC iodide in NPs.[24]

3.3 Photostability of HITC-FITC NPs under UV-light

Photostability of fluorophores in HITC-FITC NPs was tested by exposure under UV-light for 2 hours duration, and fluorescence intensity at FITC and HITC iodide was measured every 30 minutes.[25,26] Source of UV light is from Stratagene 2040 EV Transilluminator (Cambridge Scientific, Watertown, MA) with 120 Volts, 60 Hz, 1.5A. Both HITC-FITC NPs, mixture of single fluorophore (HITC-NPs and FITC-NPs) were tested. Free FITC and HITC iodide dye were used as control. In order to have same medium as NPs in water, FITC-acrylate was dissolved first in DMSO and diluted with water, while HITC iodide was dissolved in THF then diluted in water.

3.4 Aqueous-stability test of HITC-FITC NPs

Purified HITC -FITC NPs was diluted to concentration of 10 mg/ml, then was stored in a 96 well plate along with free FITC and HITC dye. Sample was completely covered to avoid light and solvent evaporation and was stored at 4°C. Fluorescence intensity of both HITC-FITC NPs and free dyes (FITC and HITC) were measured and adjusted to have similar intensity at the beginning. And it was monitored and measured in 0, 1, 3 and 5 weeks of incubation.[27]

3.5 Colloidal stability of HITC-FITC NPs in protein

The colloidal stability of HITC-FITC NPs in protein was determined as described previously.[28] Purified was diluted with distill water to have concentration of 10 mg/ml. 3ml of this NPs solution was incubated with 3ml of 10% Fetal Bovine Serum in 1x PBS to have final volume

of 6ml. HITC-FITC NPs in distill water was used as experimental control. Both sample and control were incubated at 37 °C in Shake 'N Bake™ Rocking Hybridization Oven 136400 (Boekel Scientific, Feasterville, PA). NPs' size change was monitored at 0, 6, 12, 24 and 48 hours of incubation using DLS.

4. In vitro study

Different cell lines include KYSE-30 (human esophageal cancer was a gift from Dr. Zui Pan at University of Texas at Arlington), NIH 3T3 (murine fibroblast), Raw 264.7 (murine macrophage) and Tramp C2 (murine prostate cancer), all were purchased from ATCC (Manassas, VA), have been used to examine cell compatibility and labeling efficiency of the HITC -FITC NPs.

KYSE 30 esophageal cancer cells were cultured in 1:1 mix of Ham's F-10 medium and RPMI medium (Thermo Fischer Scientific, Grand Island, NY) supplemented with 5% fetal bovine serum (Atlanta Biologicals, Flowery Branch, GA) and 1% Penicillin-Streptomycin (Gibco, Waltham, MA).

Tramp C2 cancer cells were cultured in DMEM 1X high glucose w/L-glutamine & w/o sodium pyruvate (Gibco, Waltham, MA) supplemented with 5% Nu-Serum IV (Collaborative Biomedical Products, Bedford, MA), 5% FBS, 5μg/ml insulin (Sigma, St. Louis, MO), 25u/ml Penicillin-Streptomycin and 10 M 5α-Androstan-17β-ol-3-one From Sigma in 100% ETOH.

NIH 3T3 and Raw 264.7 were cultured in Dulbecco's modified Eagle's medium (DMEM; Gibco) supplemented with 10% fetal bovine serum.

4.1 Compatibility study

In order to assess the cell compatibility of the particle, optimal HITC -FITC NPs, which has highest intensity in both visible and NIR range from study 2.2, was chosen for cell study.

To this purpose, KYSE-30 and Tramp C2 were treated with different concentration of HITC- FITC NPs for 24 hrs. The cells viability was evaluated using the Alamar Blue assay[29]. Briefly, 10,000 cells were seeded in 96 well plate and treated with different concentration of HITC-FITC NPs (0.003, 0.03, 0.3 and 3 mg/ml triplicate). After 24 hours the particles were removed and replaced with 100 of assay medium consisting of complete medium and 10% alamar blue (Bio-Rad Hercules, CA). After 4 h of incubation, the assay medium was collected, and the optical density was read at 570 nm and 595 nm. The viability of the cells was reported as percentage of non-treated control groups.

4.2 Cell labeling

KYSE-30, Tramp C2, NIH 3T3 and Raw 264.7 were seeded in 35mm petri dish with No. 1.5 cover glass (MatTek, Ashland, MA). After adhesion of the cells, the medium was replaced with FITC-HITC NPs (0.3 mg/ml) in cell media. After 2 hours, the media was discarded, and the image of the cells was taken using on focal laser scanning microscopy (Leica, (Leica TCS SP8 SMD, Leica, Buffalo Grove, IL, USA) at different channels: FITC (Excitation: 490nm, Emission: 525nm Exposure time: 800ms) and White light channel (Exposure time: 100ms).

5. Cell tracking –*in vivo* whole-body imaging and *in vitro* microscopic imaging study

All animal experiment protocols were approved by Animal Care and Use Committee of the University of Texas at Arlington. Cancer metastasis mice model was used to determine the ability

of HITC-FITC NPs to track esophageal cancer cell migration in vivo. For that, 1 million of KYSE-30 esophageal cancer cells were harvested and labeled with HITC-FTIC-NPs (300 ug/ml). HITC -FITC-NPs labeled esophageal cancer cells were administered intravenously into the animals. In vivo cell accumulation was monitored for 3 days using Kodak In-Vivo Imaging System FX Pro (Carestream Health Inc., New Haven, CT, USA) as described previously.[30] At the end of the study, cell biodistribution was performed and histological analysis was carried out as previously described.[31] 10 um thick of cryosections were made and microscopic images were taken utilizing a Leica fluorescence microscope (Leica Microsystem GmbH, Wetzlar, Germany) combined with a Retiga-EXi CCD camera (QImaging, Surrey, BC, Canada).

6. Statistical analysis

All the data were evaluated using two-tailed student t-test and presented as mean ± standard deviation. Statistical analyses of all data were performed by a Student t-test. The results showed significance when p value < 0.05. All tests were conducted in triplicate for statistical analysis.

Result and Discussion

1. Characterizations of HITC-FITC NPs

1.1 Physical characteristic of HITC-FITC NPs

To prepare dual dyes loaded NPs, FITC fluorophore was chemically incorporated in the particle during polymerization method. Amount of FITC-acrylate added was optimized first to exhibit the highest fluorescence intensity as well as suitable particle size (Figure 1 and **Error! Reference source not found.**). In order to produce HITC-FITC NPs, HITC was incorporated into the particle

by physical entrapment. Size and morphology of the particle before and after loading of HITC iodide dye was monitor (Figure 2 and Figure 3). There was no significant difference in particle size and morphology between FITC NPs and HITC-FITC NPs; thus HITC loading does not affect NPs physical characteristics. This ability to swell and shirk back of the particles is possibly due to solubility parameter of polymer in different polar solvents. In other words, cross linker, DVB has the ability to either relax in THF or restrain in water.[32] Consequently, this ability makes tight physical encapsulation of HITC inside the particle possible. HITC-FITC NP has a round shape with average size of 142.9nm±2.2, while size distribution is slightly skewed to the left.

1.2 Chemical characteristic of HITC-FITC NPs

FTIR was performed to confirm NPs' chemical composition and identify each reagent's presence (Figure 5**Error! Reference source not found.**). Peak between 3650 and 3200 cm^{-1} confirm the presence of alcohol's O-H bond from HEMA, while peak at 3300-2500 cm^{-1} shows the presence of acrylic acid's O-H bond. Peak at 1250-1050 cm^{-1} is due to C-O single bond, as well as peak with strong intensity at 1780-1650 cm^{-1} is a characteristics of C=O double bond which is from HEMA and FITC-acrylate. There's also a strong signal in 1500-1430 cm^{-1} from benzene ring from styrene.[33]

To improve particles' colloid stability as well as allowing further surface modification, acrylic acid was conjugated into the particle. To quantify the amount of carboxyl group on NPs' surface, conductivity titration was performed. Mole of carboxyl group was calculated through two equivalent points of titration curve (Figure 4). There's 0.276 mmole of carboxyl group per gram of NPs, this contributes the negative zeta potential (-14.46mV) of NPs.

1.3 Optical characteristic of HITC-FITC NPs

To optimize optical property in NIR and visible range, FITC-NPs was labeling with various amount of HITC iodide (Figure 7) and their intensity were analyzed by fluorescence microplate reader. Emission scan (Figure 7) confirms presence of both FITC and HITC iodide fluorophores within the NPs. In visible range, HITC -FITC NPs has emission peak at 510 nm comparing to free FITC's emission peak at 520nm. Similarly, in NIR range, NPs has emission peak at 796nm comparing to free HITC iodide's emission peak at 784nm. The slight shift of the spectra of both fluorophores in NP's environment is possibly dues to solvent effect[34] (Figure 6). Water was used as solvent in synthesis process thus purified HITC-FITC NPs was solely present in water during fluorescence measurement. Whereas, free fluorophores, FITC-acrylate and HITC iodide are not soluble in water, thus they have to dissolve in compatible solvents then dilute in water, DMSO for FITC-acrylate and THF for HITC. Thus, different in solvent's polarity could shift fluorescence spectrums of FITC and HITC.

According to **Error! Reference source not found.**B, FITC intensity shows a negative slope as r aising HITC iodide dosage, while HITC intensity exhibit a peak at ratio of 0.4 x10-3 w/w%. Comparatively, HITC-FITC NPs is shown to have high HITC loading efficiency (>90%) (**Error! R eference source not found.**). Loading efficiency of HITC increases with amount HITC used. Therefore, even though there's more HITC iodide presents inside NPs, the intensity tends to reduce, which suggest self-quenching.[35] On the other hand, FITC intensity is inversely proportional to loading efficiency of HITC iodide. One might suggest dynamic quenching. However, dynamic quenching only occurs when there's overlap of fluorophores' fluorescence spectrum. In this case, spectrums of FITC and HITC iodide is ~100nm apart, thus the gap is too long for dynamic quenching to efficiently occurs.[36,37] One possible explanation for this observation

is static quenching, at which fluorophore, FITC, and its quencher, HITC iodide, form a complex that does not have fluorescence intensity.[38] Thus, as quencher concentration increases, complex concentration increase, and active fluorophore decreases thus the intensity is reduced. However, FITC is shown not to have to same effect on HITC intensity. Nevertheless, HITC-FITC NPs with ratio of 0.4 $x10^{-3}$ w/w% was selected as optimal nanoprobes for *in vitro* and *in vivo* studies and further analysis.

1.4 Stability of HITC-FITC NPs

To investigate photostability of the probes, HITC-FITC NPs were undergoing accelerated decayed by exposed to UV light and change in fluorescence intensity was monitored, along with free FITC, HITC and mixture of single dye NPs (Figure 8). Free HITC iodide was decaying at faster rate comparing to both dual and single HITC iodide NPs. At the end of 2 hours, free HITC iodide decayed completely, while in HITC-FITC NPs, intensity is only reduced by 20%. Since HITC is encapsulate inside the nanoparticle, the polymer matrix of the particles possibly protect HITC from oxygen and UV radiation, thus significantly reduce its degradation rate.[39, 40] On the other hand, with FITC fluorophore, intensity increases by 1.5-folds in HITC-FITC NPs after 2-hour UV irradiation, while slightly remains constant in free dye and single dye NPs. This change in intensity possibly causes by reduction in static quenching between HITC iodide and FITC fluorophore. Since as previously mentioned, physical contact between FITC and HITC iodide causes them to form a complex which does not have fluorescence intensity at FITC range. Thus, as HITC iodide decays over time, the concentration of this complex decreases and release FITC thus as concentration of FITC increases, its intensity also increases. Whereas, in mixture of single dye particle, the physical contact between two fluorophores was not presented thus the intensity remains constant as in free FITC-acrylate.

Lifetime of this particle was also performed to test aqueous stability of NPs in normal storage condition, which is at 4°C for over 5 weeks (Figure 9**Error! Reference source not found.**). Free FITC-acrylate and NPs form were highly stable during 5 weeks' period. On the other hand, HITC iodide intensity in NPs reduced by 9%, while free HITC iodide dye decayed 98% by the end of 5th week. This result suggests particle composition stabilizes both FITC and HITC iodide fluorophores and extend its lifetime.[41]

To predict its behavior in cell environment, colloid stability of HITC-FITC NPs in protein media was tested (Figure 10). HITC-FITC NPs were incubated with serum/PBS mixture and particle size change was monitor. Comparing to control NPs that incubated in water, there's no significant difference size ($p \leq 0.1$) (**Error! Reference source not found.**A). Thus, HITC-FITC N Ps are stable in presence of protein, suggesting that the probe may be used to stain cells for *in vitro/in vivo* application.

2. In vitro study

To investigate cytotoxicity of the FITC-HITC NPs to cells, Alamar blue assay was used to evaluate cell viability based on the reduction potential of metabolically active cells. The cell viability is reported as percentage of the reduction of each group compared to the control group without any treatment as shown in **Error! Reference source not found.**B (Figure 10). No significant signs of t oxicity were observed for different concentration of FITC-HITC NPs up to 0.3 mg/ml. The results show that cell treatment with 3 mg/ml of FITC-HITC for 24 hours has significant effect on cell proliferation and viability of the KYSE-30 and Tramp C2 cells ($p \leq 0.01$).

To investigate ability of the HITC -FITC NPs to label cells, 4 different types of cell (namely, KYSE-30 human esophageal cancer cells, Tramp C2 murine prostate cancer cells, NIH 3T3 murine fibroblast cells and murine Raw 264.7 macrophage) were employed. The results presented in

Figure 11 show that all four types of cells are successfully labeled with FITC-HITC NPs and can be easily observed under a fluorescent microscopy, suggesting that the HITC -FITC NPs that may label different cell from different tissues and organism.

3. In vivo study

In vitro test shows that esophageal cancer cells can be labeled with HITC -FITC NPs. We further investigate migration profile of the cancer cells in murine cancer model using an in vivo NIR imaging system. For that, 1 millions of esophageal cancer cells (KYSE-30) labeled with HITC -FITC NPs were injected intravenously from retro-orbital vein. Three days later, cancer cells can be detected in vivo under a NIR channel (excitation: 760nm and emission: 830nm) (Figure 12). The high intensity and great affinity of dye in cancer cells allows us to monitor cell accumulation for several days.

On the third day, biodistribution was executed to confirm the cell accumulation (Figure 13). Most of labeled cells moved to liver while the rest of cells occupied in spleen and lung.

Histology was utilized to investigate the cellular level of labeled cancer cells. 10 um thick of lung sections were made and images of sections were taken under FITC (HITC -FITC NPs, green) and DAPI (nucleus, blue) channels. Merged pictures shows that cancer cells invaded into lung and the intensity of FITC can be detected even though less cancer cells migrated to lung (Figure 14).

Conclusion

Two fluorescence agents, FITC and HITC iodide were successful incorporated into nanoparticle, which exhibits high fluorescent intensity at both visible and NIR ranges. Comparing to free agents, HITC-FITC NPs exhibits significantly higher photostability, aqueous and colloid stability. These nanoparticles are compatible with different types of cell, esophageal and prostate cancer cells,

fibroblast cells and macrophages. In other word, HITC-FITC-NPs can be used for cell labeling with high intensity thus give high imaging contrast while also exhibit low cytotoxicity. HITC-FITC NPs-labeled esophageal cancer cells were administered intravenously in animals. After implantation for 72 hours, our results confirm that we are able to track cell migration and distribution in various organs using *in vivo* whole-body and *in vitro* microscopic imaging, respectively. Therefore, these results support that our HITC-FITC NPs can be used as a cell labeling agent for both whole body and microscopic imaging applications.

Other researchers also have developed nanoprobe which allow both *in vitro* and *in vivo* imagine,[42] however their focus is for determining tissue depth, thus biocompatibility was not their main critique. Whereas our nanoprobe are highly compatible with cells thus exhibit higher sensitivity in cell labeling. More importantly, this nanoprobe also allows cell imaging in both cell labeling in vitro, cell migration in vivo as well as subsequent histology, consecutively. This does not only simplify experimental procedure but also provide high imaging contrast in both *in vitro* and *in vivo* imaging field. Furthermore, by utilizing the existing carboxyl group on the NPs' surface, targeting moiety can be conjugating to improve specificity.

Appendix A: Figures

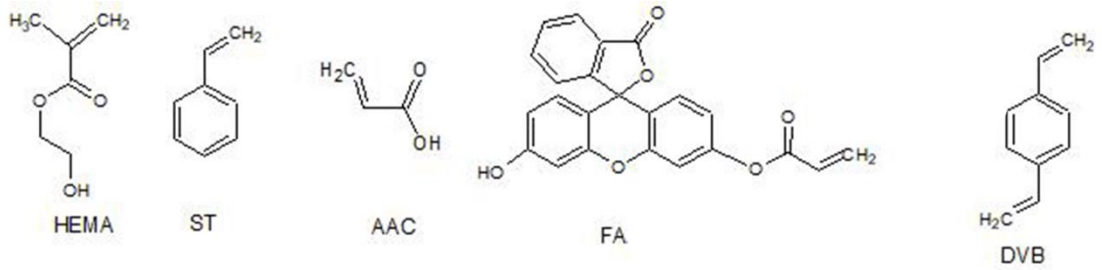

Scheme 1*: Reagents used in FITC-NPs synthesis process.*

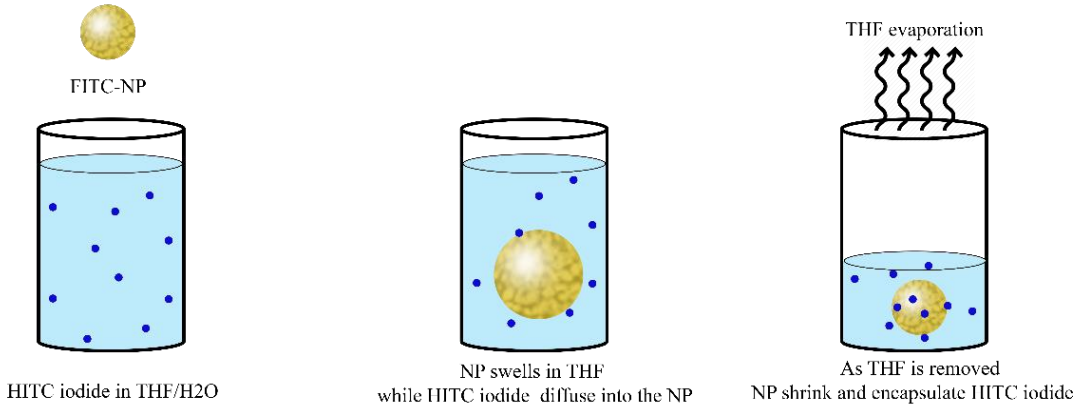

Scheme 2: Encapsulation procedure of HITC iodide into FITC-NPs via swelling effect. Purified FITC-NPs was incubated in H2O and THF in present of HITC dye molecules. Due to solvent effect, FITC-NPs is swelled, allow HITC iodide to diffuse into the particle. As THF is removed by evaporation, FITC-NPs shirked back to its original size and trap HITC iodide inside, to produce HITC-FITC-NPs.

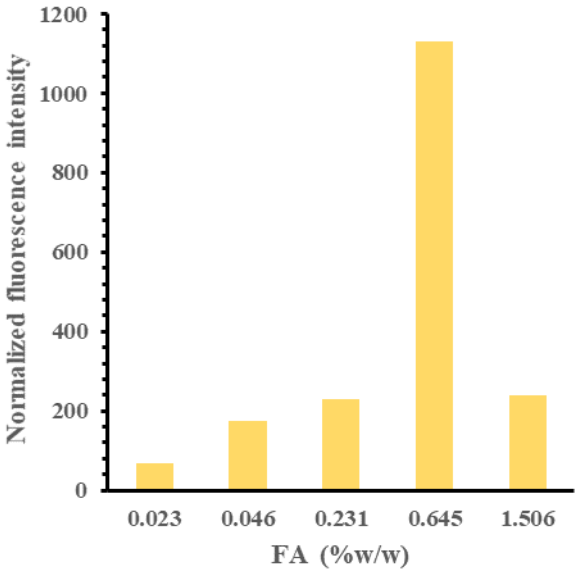

FA (%W/W)	PARTICLES SIZE (NM)
0.023	92.1±28.3
0.046	94.6±22.4
0.231	100.3±30.7
0.645	146.8±3.73
1.506	98.1±19.9

Figure 1(left): Fluorescence intensity of different FITC NPs were synthesized with same reagents and amount as mentioned in method 1.1, except with vary amount of FITC-acrylate. All samples were prepared in water, and intensity was normalized by concentration.

Table 1(right): Size of different FITC NPs

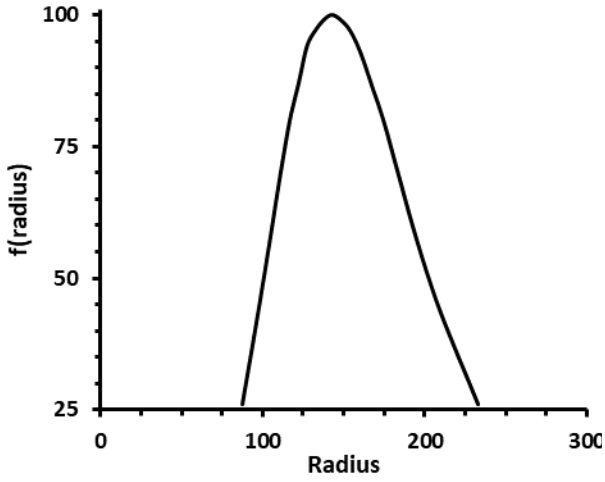

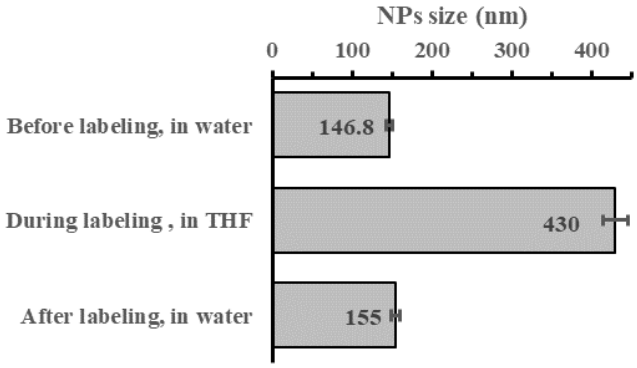

Figure 2: A) Size distribution of HITC-FITC NPs. B) Size change during HITC encapsulation

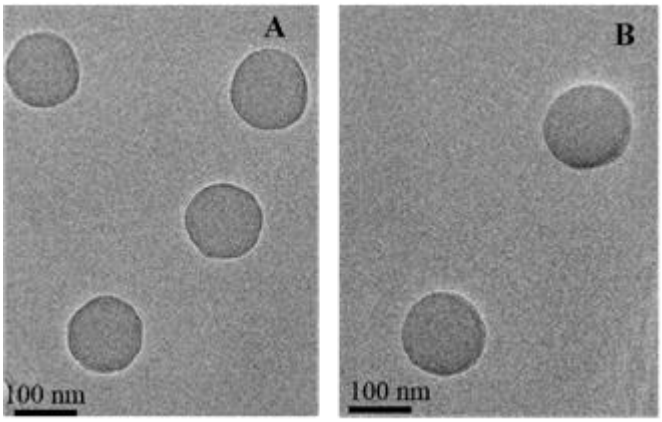

Figure 3: TEM image of A) FITC NPs. B) HITC-FITC NPs

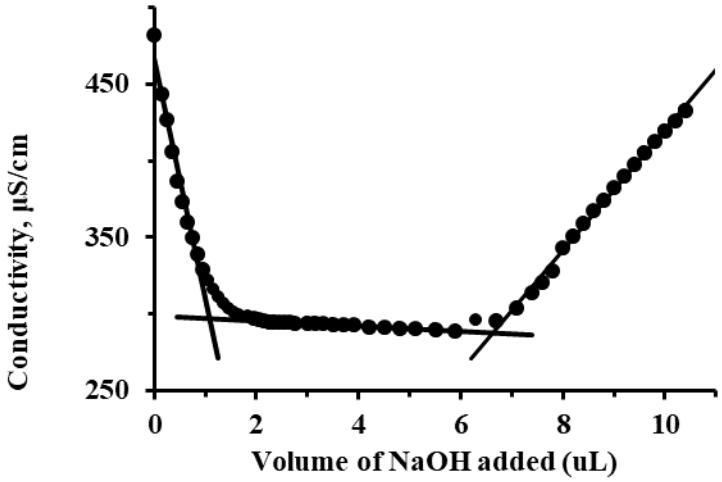

Figure 4: Conductivity titration curve of FITC-NPs for carboxyl group quantification. Equivalence point 1 is the volume of NaOH that require for strong acid (HCl). Equivalence point 2 is total volume to titrate strong acid and weak acid (carboxyl group). By calculate the different and convert through molarity, mole of carboxyl groups presents on particle's surface.

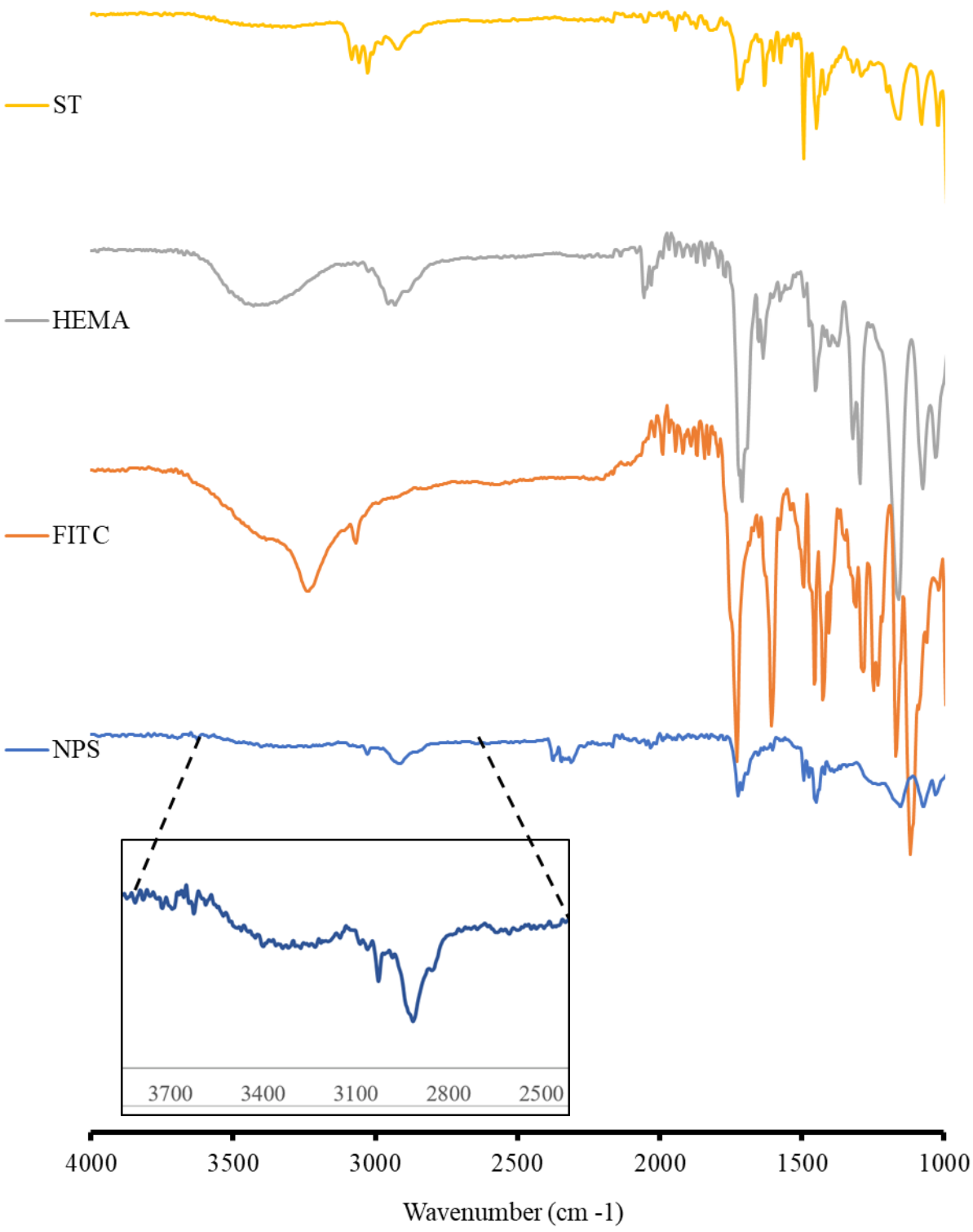

Figure 5: FTIR spectra of FITC-NPs and reagent monomers.

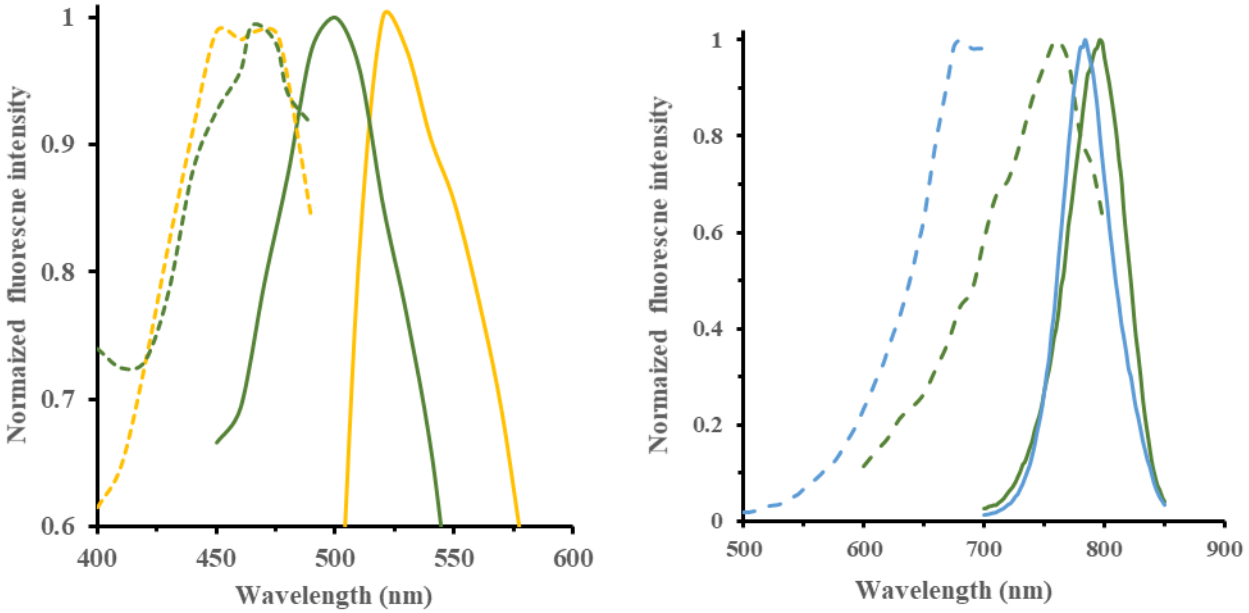

Figure 6: Full fluorescence spectrum of HITC-FITC-NPs at IR and FITC with free fluorophores. Orange: Free FITC in DMSO/H2O, blue: Free IR750 in THF/H2O, green: IR-FITC-NPs in H2O. Solid line: Emission, dot line: Excitation.

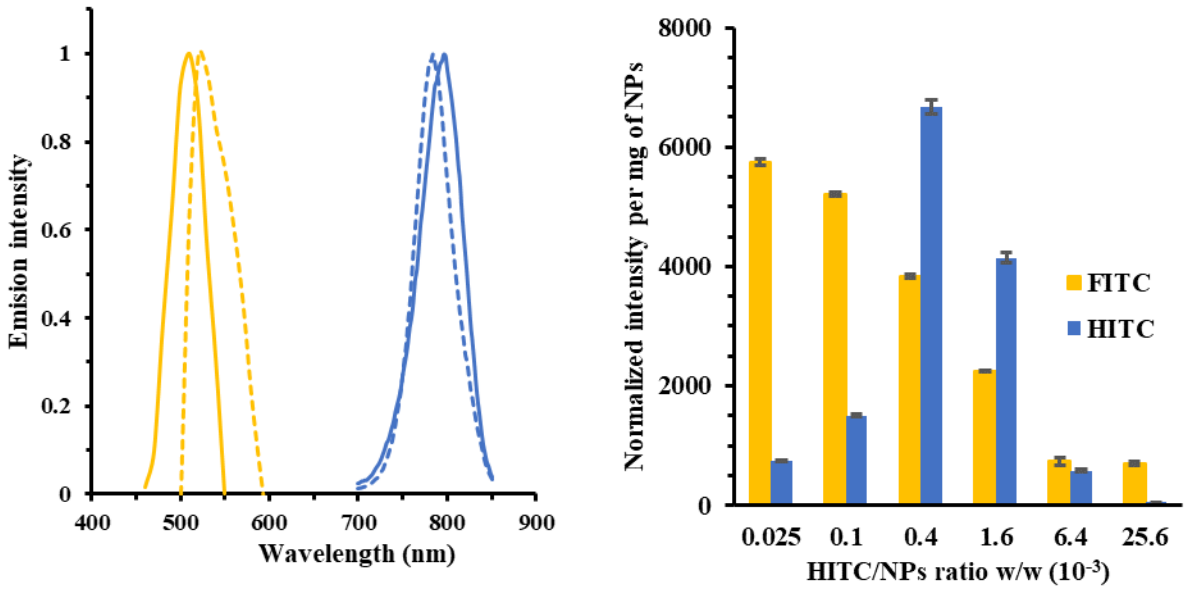

Figure 7: A) Emission fluorescence spectrum of HITC-FITC NPs and free fluorophores. Yellow: emission of FITC fluorophore, blue: emission of HITC fluorophore. Solid line: HITC-FITC NPs, dotted line: free fluorophore. B) Fluorescence intensity in visible and NIR range of HITC-FITC NPs vs. different amount of HITC added during encapsulation. All sample were prepared in water. Intensity was normalized by particle concentration.

Dye/NP ratio (10E-3 %w/w)	Microgram of HITC iodide loaded per gram of NPs	% loading
0.025	1.15±0.070	91.79
0.1	4.93±0.068	98.62
0.4	19.89±0.074	99.44
1.6	79.91±0.071	99.89
6.4	319.91±0.069	99.97
25.6	1279.91±0.069	99.99

Table 2: Loading efficiency of HITC in FITC NPs

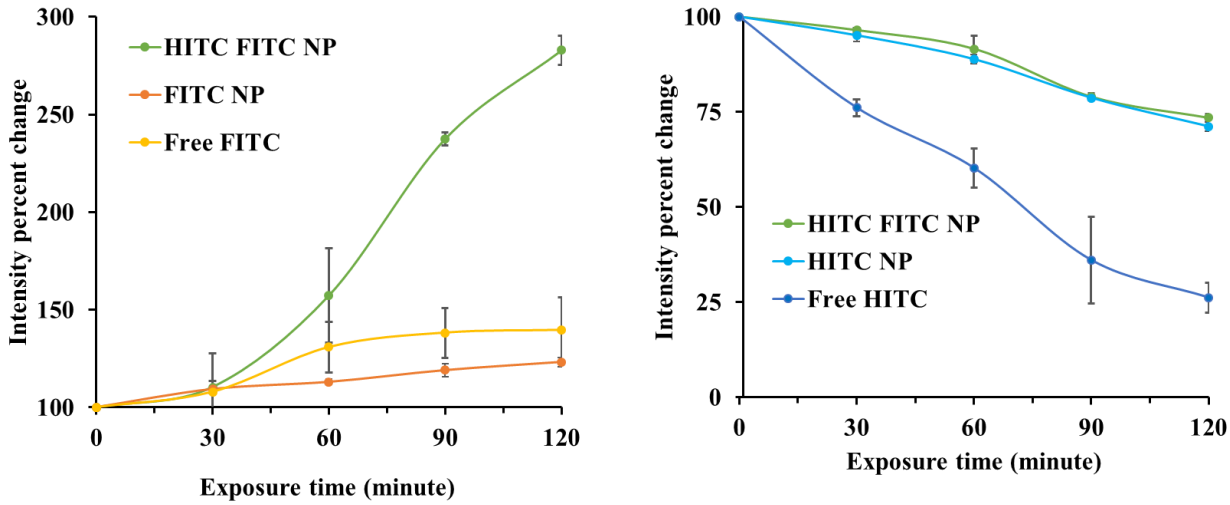

Figure 8:Photostability. Utilizing UV light exposure, photostability of HITC -FITC NPs and free fluorescence agents was monitoring at A) HITC range (Excitation: 760nm, Emission: 796nm). B) FITC range (Excitation: 470nm, Emission: 510nm).

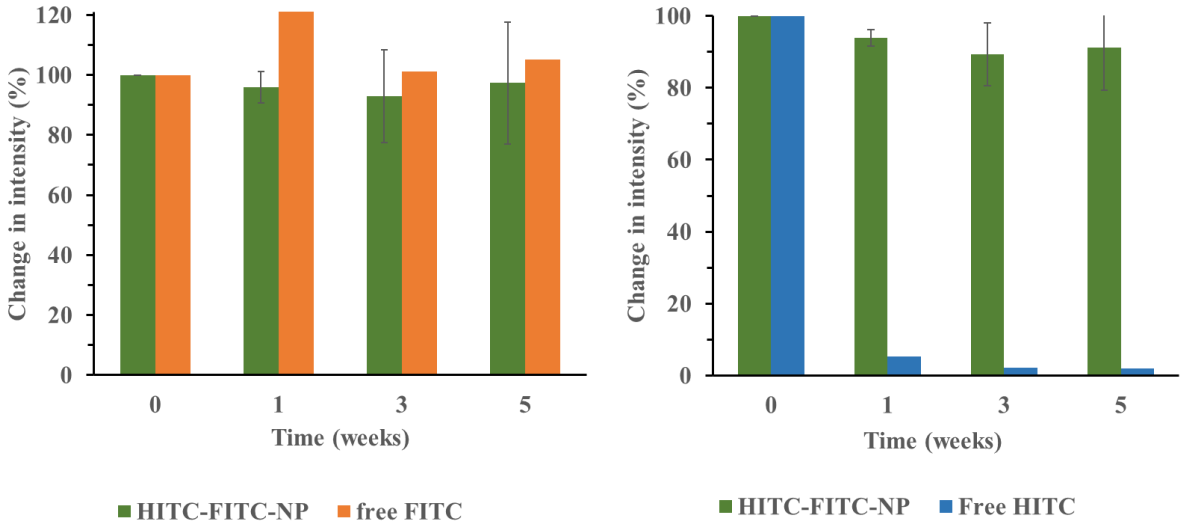

Figure 9: Aqueous stability. HITC-FITC NPs were stored in 4ºC in closed environment to avoid light and solvent evaporation, and fluorescence intensity was frequently monitor at A) HITC range (Excitation: 760nm, Emission: 796nm). B) FITC range (Excitation: 470nm, Emission: 510nm).

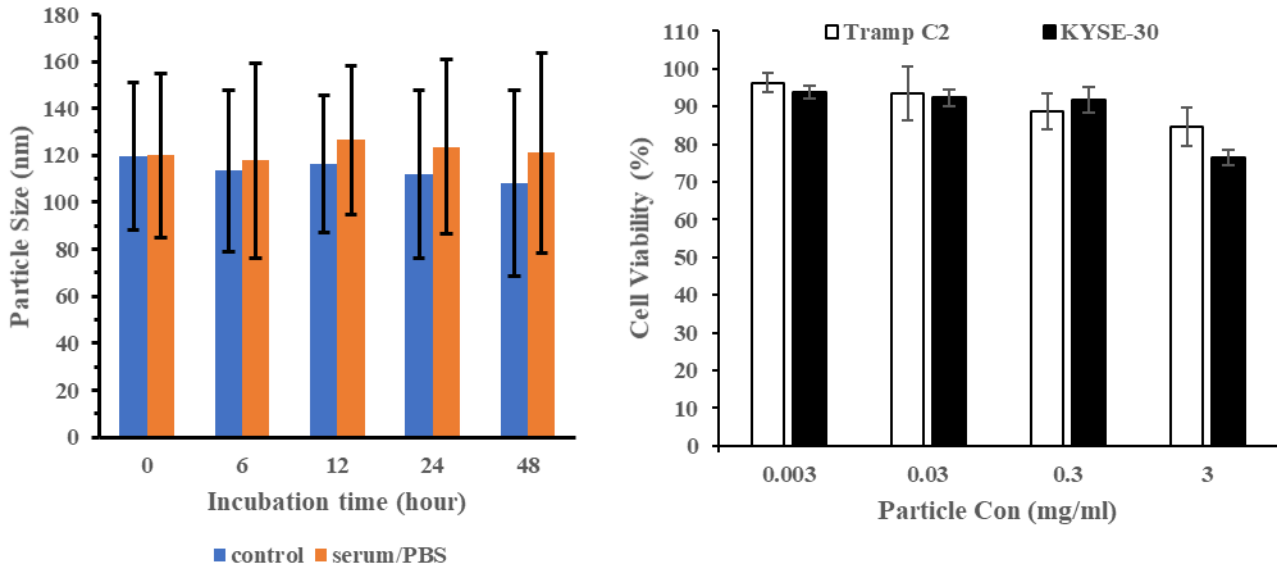

Figure 10: A) Colloid stability in protein serum. B) Cytotoxicity in Tramp C2 and KYSE-30 cells of HITC-FITC-NPs

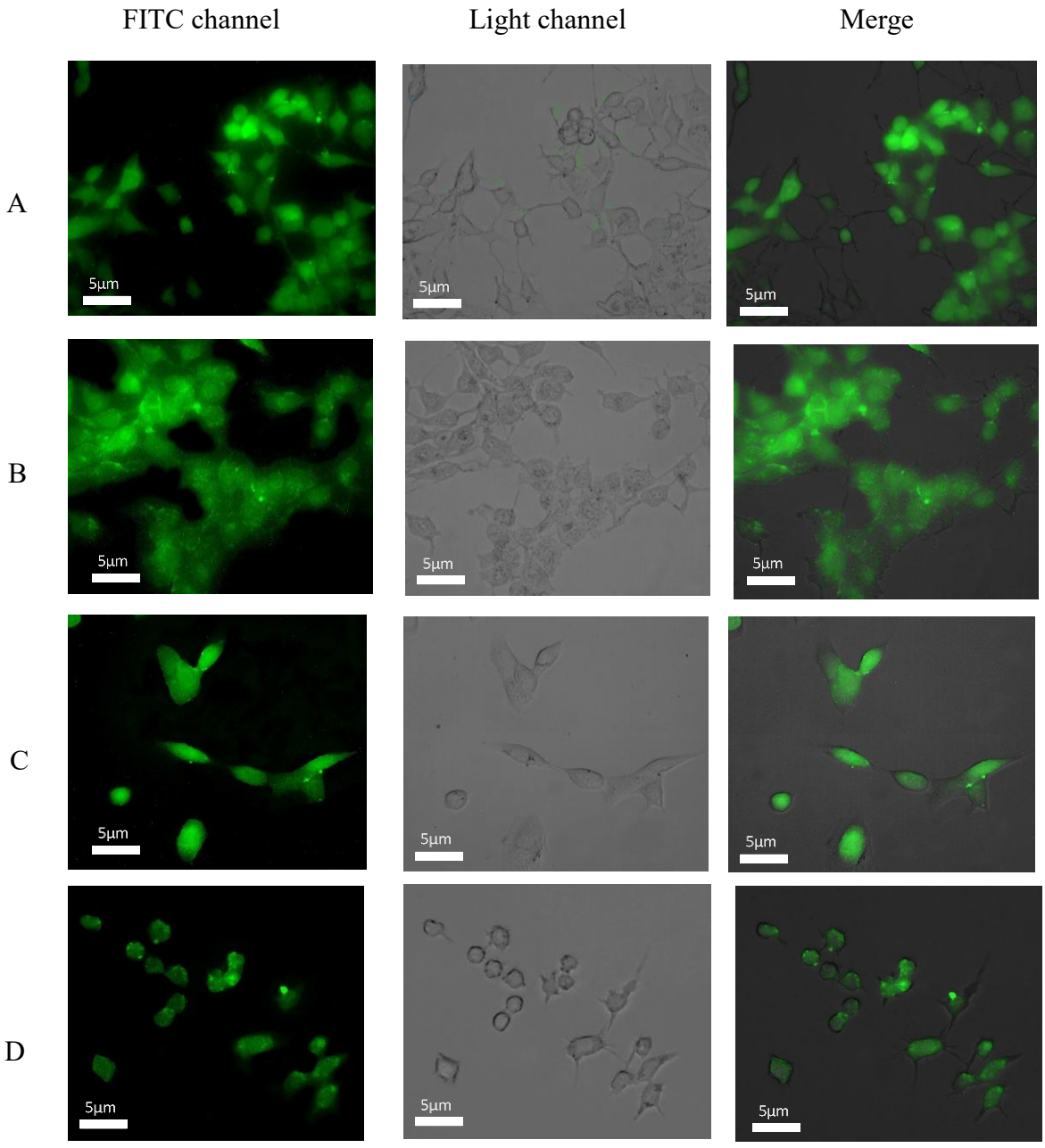

Figure 11: Different types of cell labeled with HITC-FITC-NPs in FITC channel. A: KYSE 30 cells. B: Tramp C2. C: NIH 3T3. D: Raw 264.7.

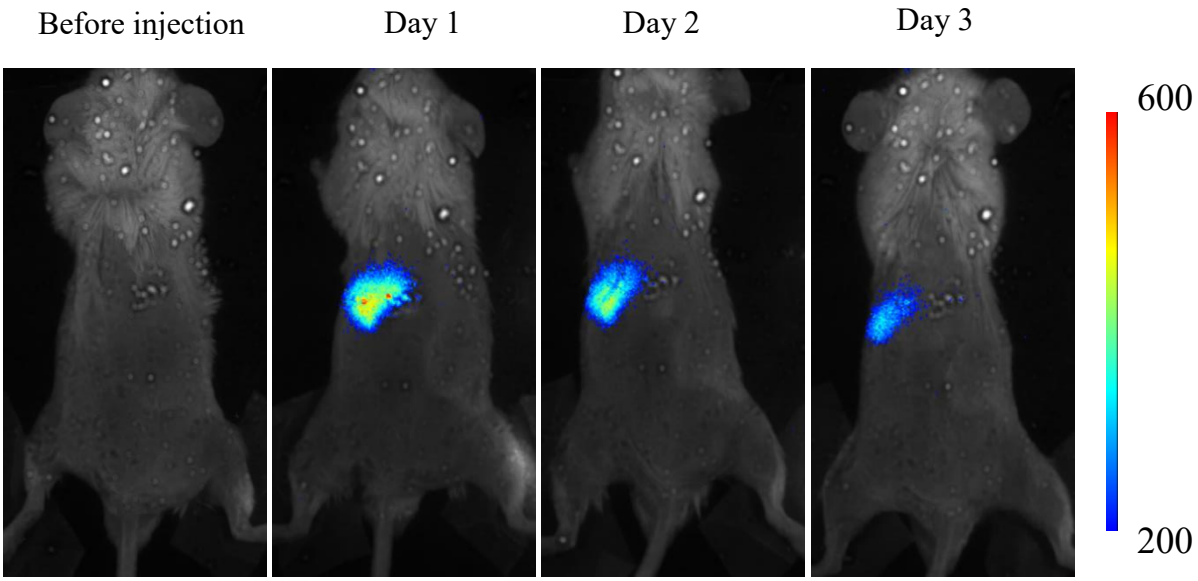

Figure 12: HITC-FITC NPs labeled esophageal cancer cells (KYSE-30) were monitored using Kodak In-Vivo Imaging System for 3 days. Cells accumulated near left ribs of the mouse.

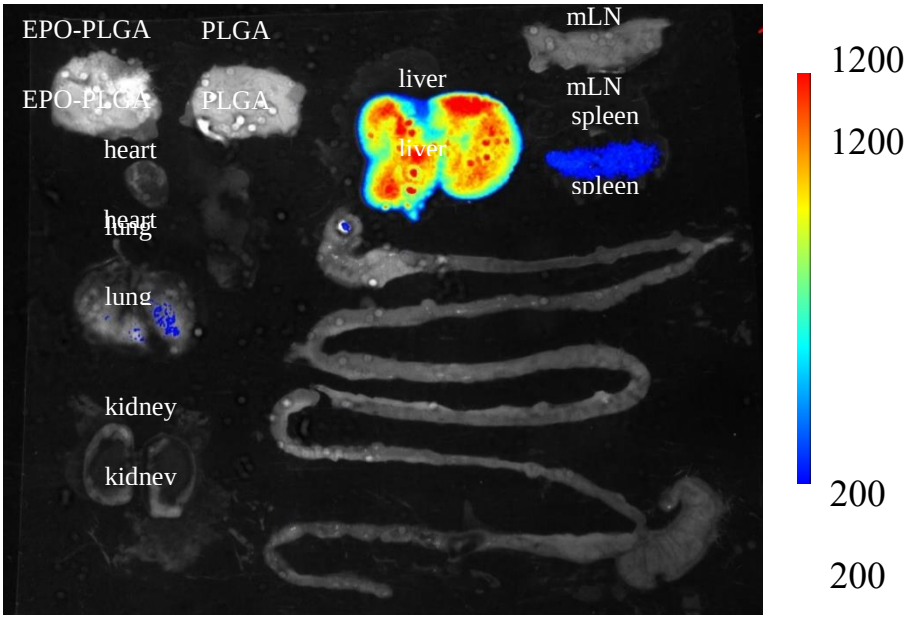

Figure 13: For biodistribution test, most of the NPs labeled cancer cells accumulated at the liver while some deposit in the spleen and the lung after 3 days. Both of in vivo images and biodistribution were taken with excitation wavelength at 760nm and emission wavelength at 830nm.

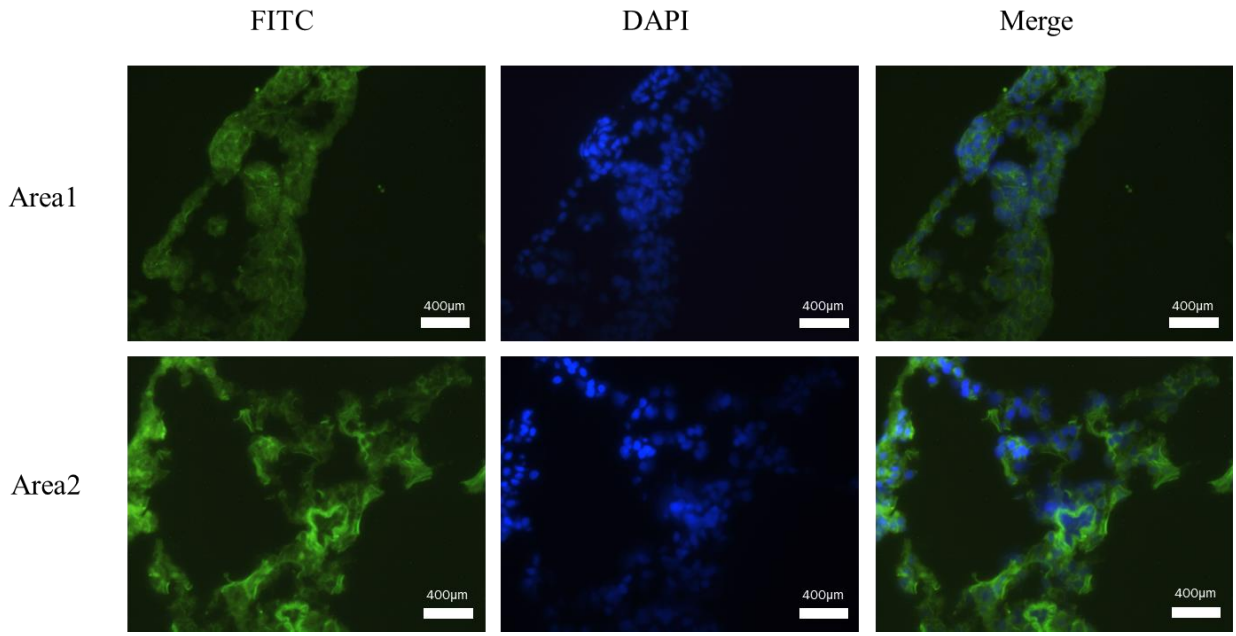

Figure 14: Fluorescent microscope images of lung sections were taken under FITC (NPs, green) and DAPI (nucleus, blue) channels.

Appendix B: Background calculation

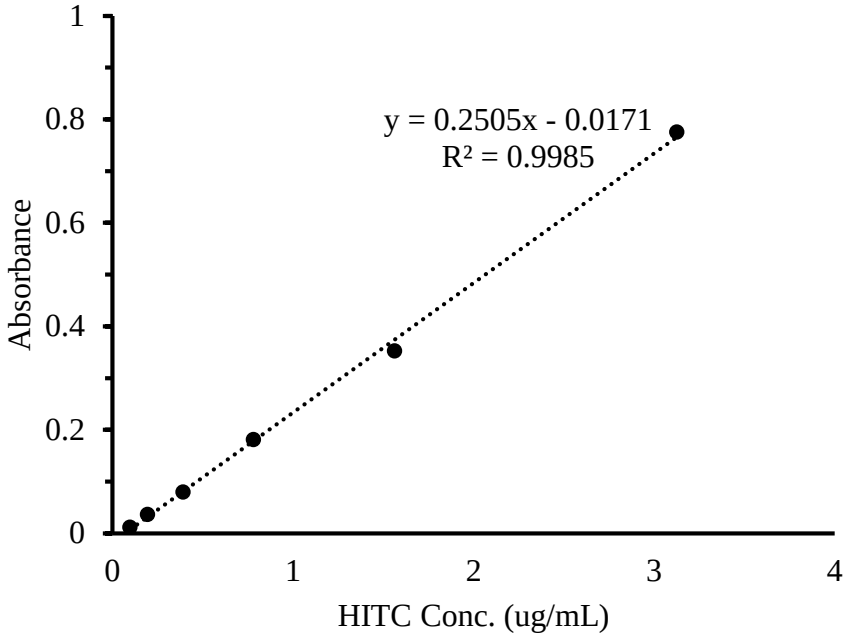

Figure A1: Standard curve of HITC iodide for loading efficiency calculation

Dye/NP ratio (10E-3)	Average Abs	Conc. (ug/ml)	HITC iodide in unit of ug			%loading
			unloaded	loaded	added	
0.025	0.0086	0.103	0.51	0.74	1.25	58.96
0.1	0.0002	0.069	0.35	4.65	5.00	93.08
0.4	0.0108	0.11	0.56	19.44	20.00	97.22
1.6	0.0052	0.089	0.44	79.56	80.00	99.44
6.4	0.0064	0.094	0.47	319.53	320.00	99.85
25.6	0.0064	0.094	0.47	1279.53	1280.00	99.96

Table A2: Calculation of HITC loading efficiency in FITC NPs

Trial	1	2		
x intercept 1	1.714	1.0634		
x intercept 2	6.095	6.575		
V NaOH (ml)	4.381	5.5116		
mM NaOH	0.04381	0.055116		
mM carboxyl group	0.04381	0.055116	Average	STD
mmol NaOH per gram of NP	0.21905	0.27558	0.247	0.04

Table A3: quantification of carboxyl group on NPs' surface

Reference

[1] Huang, Yihui & Zhou, Jun & Hakamivala, Amirhossein & Wu, Jinglei & Hong, Yi & Borrelli, Joseph & Tang, Liping. (2017). An optical probe for detecting chondrocyte apoptosis in response to mechanical injury. Scientific Reports. 7. 10.1038/s41598-017-10653-y.

[2] Peng, Zhaoqiang & Zhou, Jun & Dacy, Ashley & Zhao, Deyin & Kearney, Vasant & Zhou, Weidong & Tang, Liping & Hu, Wenjing. (2017). Design of a portable imager for near-infrared visualization of cutaneous wounds. Journal of Biomedical Optics. 22. 016010. 10.1117/1.JBO.22.1.016010.

[3] (2018). In vivo and in situ activated aggregation-induced emission probes for sensitive tumor imaging using tetraphenylethene-functionalized trimethincyanines-encapsulated liposomes. ACS Applied Materials & Interfaces. 10.1021/acsami.8b07727.

[4] Key, Jaehong, and James F Leary. "Nanoparticles for Multimodal in Vivo Imaging in Nanomedicine." *International Journal of Nanomedicine* 9 (2014): 711–726. *PMC*. Web. 16 May 2018.

[5] Kherlopian, Armen R et al. "A Review of Imaging Techniques for Systems Biology." BMC Systems Biology 2 (2008): 74. PMC. Web. 9 July 2018.

[6] A. Kiani, A. Esquevin, N. Lepareur, P. Bourguet, F. Le Jeune, and J. Gauvrit, "Main applications of hybrid PET-MRI contrast agents: A review," Contrast Media & Molecular Imaging, vol. 11, no. 2, pp. 92–98, 2016.

[7] Nam, T., Park, S., Lee, S. Y., Park, K., Choi, K., Song, I. C., ... Jeong, S. Y. (2010). Tumor targeting chitosan nanoparticles for dual-modality optical/MR cancer imaging. Bioconjugate Chemistry, 21(4), 578-582. DOI: 10.1021/bc900408z

[8] Sandra J. Rosenthal, Jerry C. Chang, Oleg Kovtun, James R. McBride, Ian D. Tomlinson,Biocompatible Quantum Dots for Biological Applications, Chemistry & Biology, Volume 18, Issue 1, 2011, Pages 10-24, ISSN 1074-5521, https://doi.org/10.1016/j.chembiol.2010.11.013.
(http://www.sciencedirect.com/science/article/pii/S1074552110004497)

[9] Zongwen Jin, Niko Hildebrandt, Semiconductor quantum dots for in vitro diagnostics and cellular imaging, Trends in Biotechnology, Volume 30, Issue 7, 2012, Pages 394-403, ISSN 0167-7799, https://doi.org/10.1016/j.tibtech.2012.04.005.
(http://www.sciencedirect.com/science/article/pii/S016777991200056X)

[10] Arranz, Alicia, and Jorge Ripoll. "Advances in Optical Imaging for Pharmacological Studies." Frontiers in Pharmacology 6 (2015): 189. PMC. Web. 9 July 2018.

[11] Lin, Michael Z. et al. "Autofluorescent Proteins with Excitation in the Optical Window for Intravital Imaging in Mammals." *Chemistry & biology* 16.11 (2009): 1169. *PMC*. Web. 16 May 2018.

[12] Macoura Gadji, Rhea Vallente, Ludger Klewes, Christiaan Righolt, Landon Wark, Narisorn Kongruttanachok, Hans Knecht, Sabine Mai, Nuclear Remodeling as a Mechanism for Genomic Instability in Cancer, Editor(s): David Gisselsson, Advances in Cancer Research, Academic Press, Volume 112, 2011, Pages 77-126, ISSN 0065-230X, ISBN 9780123876881, https://doi.org/10.1016/B978-0-12-387688-1.00004-1.

[13] Involvement of the LSPR Spectral Overlap for Energy Transfer between a Dye and Au Nanoparticle. Mani Prabha Singh and Geoffrey F. Strouse. Journal of the American Chemical Society 2010 132 (27), 9383-9391
DOI: 10.1021/ja1022128

[14] Zhang, Sheng-hua & Cheng, Xin & Zhong, Gen-shen & Xiong, Dong-sheng & Shao, Rong-guang. (2010). In vivo imaging analysis of biodistribution of FITC-labeled Rituximab in lymphoma-bearing nude mice. Zhonghua yi xue za zhi. 90. 2367-70. 10.3760/cma.j.issn.0376-2491.2010.33.018.

[15] S. Ramachandran, S. Thiyagarajan, G. Dhinakar Raj, A. Uma, Non-invasive in vivo imaging of fluorescence-labeled bacterial distributions in aquatic species, International Journal of Veterinary Science and Medicine, Volume 5, Issue 2, 2017, Pages 187-195, ISSN 2314-4599,

[16] Xinxin Zhu, Hui Jin, Cuili Gao, Rijun Gui, Zonghua Wang, Ratiometric, visual, dual-signal fluorescent sensing and imaging of pH/copper ions in real samples based on carbon dots-fluorescein isothiocyanate composites, Talanta, Volume 162, 2017, Pages 65-71, ISSN 0039-9140,
https://doi.org/10.1016/j.talanta.2016.10.015.

[17] Papineni, Rao, et al. Fluorescence Resonance Energy Transfer Detection with Nanoparticles for in Vitro and in Vivo Applications. 23 Sept. 2014.

[18] Tang EN, Nair A, Baker DW, Hu W, Zhou J. In Vivo Imaging of Infection Using a Bacteria-Targeting Optical Nanoprobe. Journal of biomedical nanotechnology. 2014;10(5):856-863.

[19] Behnke, Thomas & Würth, Christian & Hoffmann, Katrin & Hübner, Martin & Panne, Ulrich & Resch-Genger, Ute. (2010). Encapsulation of Hydrophobic Dyes in Polystyrene Micro- and Nanoparticles via Swelling Procedures. Journal of fluorescence. 21. 937-44. 10.1007/s10895-010-0632-2.

[20] Wu, Xiao, et al. "Preparation and in vitro evaluation of topical formulations based on polystyrene-poly-2-hydroxyl methacrylate nanoparticles." *Molecular pharmaceutics* 6.5 (2009): 1449-1456

[21] Olga Sambalova, Kerstin Thorwarth, Norbert Victor Heeb, Davide Bleiner, Yucheng Zhang, Andreas Borgschulte, and Alexandra Kroll ACS Omega 2018 3 (1), 724-733 DOI: 10.1021/acsomega.7b00982

[22] Wu X, Griffin P, Price GJ, et al. Preparation and in vitro evaluation of topical formulations based on polystyrene-poly-2-hydroxyl methacrylate nanoparticles. Mol Pharm. 2009;6(5):1449–1456.

[23] Fras, Lidija, et al. "Quantitative determination of carboxyl groups in cellulose by complexometric titration." *Lenzinger Berichte* 81 (2002): 80-88.

[24] Mohammadpour Dounighi, N., et al. "Preparation and in vitro characterization of chitosan nanoparticles containing Mesobuthus eupeus scorpion venom as an antigen delivery system." Journal of Venomous Animals and Toxins Including Tropical Diseases 18.1 (2012): 44-52.

[25] C.C. Chen, C.S. Lu, Y.C. Chung, J.L. Jan, UV light induced photodegradation of malachite green on TiO2 nanoparticles, Journal of Hazardous Materials, Volume 141, Issue 3, 2007, Pages 520-528, ISSN 0304-3894, https://doi.org/10.1016/j.jhazmat.2006.07.011.

[26] Santra, Swadeshmukul, et al. "Development of novel dye-doped silica nanoparticles for biomarker application." Journal of biomedical optics 6.2 (2001): 160-167.

[27] McNamara, Kerry P., and Zeev Rosenzweig. "Dye-encapsulating liposomes as fluorescence-based oxygen nanosensors." Analytical Chemistry 70.22 (1998): 4853-4859.

[28] Lazzari, Stefano ; Moscatelli, Davide ; Codari, Fabio ; Salmona, Mario ; Morbidelli, Massimo ; Diomede, Luisa. / Colloidal stability of polymeric nanoparticles in biological fluids. In: Journal of Nanoparticle Research. 2012 ; Vol. 14, No. 6.

[29] Ahmed, S.A., R.M. Gogal Jr, and J.E. Walsh, A new rapid and simple non-radioactive assay to monitor and determine the proliferation of lymphocytes: an alternative to [3H] thymidine incorporation assay. Journal of immunological methods, 1994. 170(2): p. 211-224.

[30] Ko, C.-Y., et al., The use of chemokine-releasing tissue engineering scaffolds in a model of inflammatory response-mediated melanoma cancer metastasis. Biomaterials, 2012. 33(3): p. 876-885.

[31] Nair, A., et al., Biomaterial implants mediate autologous stem cell recruitment in mice. Acta biomaterialia, 2011. 7(11): p. 3887-3895.

[32] M.A. Gauthier, J. Luo, D. Calvet, C. Ni, X.X. Zhu, M. Garon, M.D. Buschmann,
Degree of crosslinking and mechanical properties of crosslinked poly(vinyl alcohol) beads for use in solid-phase organic synthesis, Polymer, Volume 45, Issue 24, 2004, Pages 8201-8210, ISSN 0032-3861, https://doi.org/10.1016/j.polymer.2004.09.055.

[33] Socrates, George. Infrared and Raman characteristic group frequencies: tables and charts. John Wiley & Sons, 2001.

[34] Lakowicz J.R. (1983) Effects of Solvents on Fluorescence Emission Spectra. In: Principles of Fluorescence Spectroscopy. Springer, Boston, MA

[35] Lakowicz J.R. (1983) Quenching of Fluorescence. In: Principles of Fluorescence Spectroscopy. Springer, Boston, MA

[36] Chowdhury, Sanchari et al. “Wavelength Dependence of the Fluorescence Quenching Efficiency of Nearby Dyes by Gold Nanoclusters and Nanoparticles: The Roles of Spectral Overlap and Particle Size.” The journal of physical chemistry. C, Nanomaterials and interfaces 115.41 (2011): 20105–20112. PMC. Web. 11 July 2018.

[37] CdSe−ZnS Quantum Dots as Resonance Energy Transfer Donors in a Model Protein−Protein Binding Assay Dale M. Willard,†, Lori L. Carillo,Jaemyeong Jung, and, and Alan Van Orden. Nano Letters 2001 1 (9), 469-474

[38] Wang, Lin, et al. "Identifying structural characteristics of humic acid to static and dynamic fluorescence quenching of phenanthrene, 9-phenanthrol, and naphthalene." Water research 122 (2017): 337-344.

[39] Li, Bin & Tang, Liming & Dong, Hanpeng & Liu, Deshan & Zhou, Qixiang. (2000). Synthesis and absorption characteristics of two infrared cyanine dyes. Tsinghua Science and Technology. 5. 176-179.

[40] ishal Saxena, Mostafa Sadoqi, Jun Shao,
Enhanced photo-stability, thermal-stability and aqueous-stability of indocyanine green in polymeric nanoparticulate systems,Journal of Photochemistry and Photobiology B: Biology,Volume 74, Issue 1,2004, Pages 29-38,ISSN 1011-1344,https://doi.org/10.1016/j.jphotobiol.2004.01.002.(http://www.sciencedirect.com/science/article/pii/S1011134404000041)

[41] B Rodriguez, Victoria & M Henry, Scott & Hoffman, Allan & S Stayton, Patrick & Li, Xingde & Pun, Suzie. (2008). Encapsulation and stabilization of indocyanine green within poly(styrene-alt-maleic anhydride) block-poly(styrene) micelles for near-infrared imaging. Journal of biomedical optics. 13. 014025. 10.1117/1.2834296.
[42] Miller JP, Maji D, Lam J, Tromberg BJ, Achilefu S. Noninvasive depth estimation using tissue optical properties and a dual-wavelength fluorescent molecular probe in vivo. Biomedical Optics Express. 2017;8(6):3095-3109. doi:10.1364/BOE.8.003095.